Received: 12 January 2024 | Revised: 19 March 2024 | Accepted: 5 April 2024

DOI: 10.1002/mrm.30128

TECHNICAL NOTE

Magnetic Resonance in Medicine

Real-time imaging of decompression gas bubble growth in the spinal cord of live rats

Roman Alvarado[1,2] | **Ulrich M. Scheven**[3] | **Jens-Christian Meiners**[1,2]

[1]Department of Physics, University of Michigan, Ann Arbor, Michigan USA

[2]Department of Biophysics, University of Michigan, Ann Arbor, Michigan USA

[3]Department of Mechanical Engineering, University of Michigan, Ann Arbor, Michigan USA

Correspondence
Jens-Christian Meiners, Department of Physics, University of Michigan, 450 Church Street, Ann Arbor, MI 48109-1120, USA.
Email: meiners@umich.edu

Funding information
Divers Alert Network, Durham, North Carolina, USA

Abstract

Purpose: To observe the growth and resolution of decompression gas bubbles in the spinal cord of live rats in real time using MRI.

Methods: We constructed an MRI-compatible pressure chamber system to visualize gas bubble dynamics in deep tissues in real time. The system pressurizes and depressurizes rodents inside an MRI scanner and monitors their respiratory rate, heart rate, and body temperature while providing gaseous anesthesia under pressure during the experiments.

Results: We observed the formation of decompression gas bubbles in the spinal cord of rats after compression to 7.1 bar absolute and rapid decompression inside the MRI scanner while maintaining continuous gaseous anesthesia and vital monitoring.

Conclusion: We have shown the direct observation of decompression gas bubble formation in real time by MRI in live, anesthetized rats.

KEYWORDS

decompression sickness, gas bubble, magnetic resonance imaging, spinal cord damage

1 | INTRODUCTION

Decompression illness encompasses a broad spectrum of clinical symptoms that arise from a rapid drop in ambient pressure, most notably in sports and commercial diving,[1] caisson construction, and high-altitude aerospace operations.[2] Among the various forms of decompression illness, spinal cord decompression sickness (SC-DCS) is particularly severe, resulting in paresthesia, sensory and motor deficits, and in some cases, death.[3]

Decompression sickness is generally thought to be caused by the formation of inert gas bubbles in the body that arise from a supersaturation of the tissue with gas on a rapid reduction in the ambient pressure.[3] Aural Doppler ultrasound and 2D echocardiography have long been used to monitor the formation of circulating decompression bubbles in large veins or the heart post dive.[4] However, although these circulating bubbles are present in virtually all cases that result in DCS, their presence alone does not reliably predict DCS symptoms, and even less so the development of SC-DCS.[5] For pathophysiological studies of SC-DCS, it is, therefore, important to directly study the bubbles in the spinal cord itself instead of relying solely on readily observed circulating bubbles. Gas bubbles in the spinal cord are, up to now, only examined postmortem using pathology, which is rather limiting as it reveals no dynamic information, and it is fraught with artifacts from

fixation and slicing that are often hard to distinguish from gas bubbles.[6]

We demonstrate that it is possible to observe the formation of gas bubbles in deeper tissues directly in vivo using MRI. However, there are considerable technical challenges in combining the hyperbaric environment with MRI and maintaining anesthesia under pressure. In this proof of concept note, we present a hyperbaric chamber for small animals that is used inside an MRI scanner ($n = 2$). It can maintain gaseous anesthesia in the animal throughout the pressurization and decompression experiment, and it allows monitoring of breathing, heart rate, and temperature. Additionally, it has a heat exchanger to warm the breathing gas mixture just before entering the chamber to maintain the animal's body temperature. We present MRI data taken with this setup that show the formation of gas bubbles in the spinal cord of one of two rats in real-time on decompression from 7.1 bar absolute to normobaric conditions.

2 | METHODS

All experiments were conducted under the ethics approval of the Institutional Animal Care and Use Committee at the University of Michigan.

2.1 | MRI and pressure protocol

Images were acquired in a 7 T pre-clinical scanner (Varian, now Agilent), using a 60 mm saddle coil manufactured by Morris Instruments. Four- to 6-week-old female Sprague Dawley rats were imaged inside a custom-built MRI-compatible pressure chamber. A standard gradient echo multi-slice (GEMS) sequence was used (TR/TE = 500 ms/2.5 ms, flip angle = 30, voxel size 125 × 125 × 1000 μm^3). For this exploratory work we chose a gradient echo sequence because the images are sensitive to both spin density—the absence of spins inside a newly formed bubble—and the field distortions caused by the susceptibility contrast between the empty bubble and the tissue surrounding it. Successive image acquisitions produce a "movie" of the spinal cord with 1 min temporal resolution from frame to frame. To improve the SNR, the images acquired during compression were temporally averaged over four scans for a temporal resolution of approximately 4 min. Similarly, images acquired during decompression were temporally averaged over two scans, for a temporal resolution of approximately 2 min.

With the rat inside the pressure chamber, and the chamber placed in the scanner, the chamber was pressurized to 7.1 bar absolute in 45 s, or ~270 fsw/min. The pressure was maintained for 20 min, and then decompressed to 1 bar absolute within 30 s, or ~410 fsw/min. This protocol is known to preferentially induce neurologic DCS in rats and causes little pulmonary barotrauma because of their relatively high ventilatory rates.[7] We show several MRI scans taken from 8 min into the compression phase, to 10 min after decompression.

2.2 | Image pre-processing

The MRI images were processed using OpenCV (v. 4.8), NumPy (v. 1.26), and SciPy (1.12) algorithms programmed in Python.[8–10] To enhance image quality, each image underwent a two-fold, cubic interpolation, upsampling[10] in both dimensions. Images were registered using a phase correlation algorithm[8] that detects translational shifts in k-space. This alignment was focused on the area containing the spinal cord and vertebrae. A multi-nonlocal means denoising algorithm[8,11] was then applied using the two temporally closest scans for all images. Further noise reduction and feature edge enhancement were achieved through the implementation of a five-pixel diameter bilateral filter.[8] Last, image contrast was improved using a contrast-limited adaptive histogram equalization algorithm[8] on each image.

2.3 | Image segmentation

Following image denoising, the regions of presumptive bubble formation were determined by subtracting the average of the four initial scans from the average of the four final scans, resulting in a difference image. The distribution of the grayscale pixel intensities in the difference image was fitted with a Gaussian. Only pixels where the intensity has changed by more than two SDs were retained. Pixels outside of the spinal cord were further discarded. Contiguous pixels in this segmented image were considered as unique regions of presumptive bubble formation. An additional control region, approximately the size of the other regions, was randomly chosen at the center of the spinal cord.

Our image processing script is openly available.[12]

2.4 | Chamber and pressurization system

The cylindrical pressure chamber is machined from solid, transparent polycarbonate. The tube has a total length of 330 mm, an outer diameter of 5.74 mm, and a wall thickness of 3.3 mm. An internal polycarbonate tray supports the rat laid in a supine position. The pressure chamber tube has threads and O-ring seals on both ends to attach an end cap with electric and gas feedthroughs on one

end, and a heat exchanger for the inflowing gas on the other end. The electrical feedthroughs connect to the electrocardiography (ECG) and temperature sensors. A 5/32″ OD push-to-connect fitting connects to a pressure sensor (Dwyer Instruments 626-04-GH-P8-E2-S5) to instantaneously monitor the chamber pressure. A second fitting serves as the exit port for the anesthetic gas flow (Figure 1).

Pressure inside the pressure chamber is controlled with an electronic pressure control system. Medical-grade air, mixed with isoflurane, is compressed by a booster pump (Haskel AGD-4) to 9.3 bar absolute and stored at that pressure in a small buffer tank (Figure 1). An electronic pressure-control valve (ProportionAir QPV1MANEEZP100PSGBXN) is used in conjunction with the chamber pressure sensor and custom LABVIEW software to implement the desired pressure profiles in the chamber. An additional solenoid valve (Atlantic Valves BZW-20) is used to quickly depressurize the system, as depressurization through the control valve itself is too slow for our protocol.

2.5 | Anesthesia and vital monitoring

Because the anesthetic effect of isoflurane depends primarily on the partial pressure rather than its absolute concentration,[13] we administered an isoflurane concentration of 0.25% (v/v) to achieve stable anesthesia at 7.1 bar absolute. To simplify anesthetic maintenance at atmospheric pressure before compression and after decompression, we used a bypass valve to circumvent the booster pump and pressure control equipment during these phases of the experiment. This allowed us to directly feed the output of the evaporator into the pressure chamber at 1% (v/v) isoflurane concentration.

The pressure cell was designed to accommodate commercial MRI-compatible vital monitoring hardware from Small Animal Instruments. This monitoring suite includes the Model 1030 Monitoring and Gating Systems, 3-lead surface ECG electrodes, and a rectal thermistor to monitor the animal's temperature. Respiration is monitored using a technique termed E-RESP by Small Animal Instruments, Inc: the ECG wires are placed to make a loop around the animal's chest (Figure 2). As the loop size changes

FIGURE 2 A rat is secured on the pressure chamber tray with electrocardiography wires arranged in an E-RESP configuration, which consists of a wire looped around its chest to generate induced voltage changes from respiratory movements in the presence of a magnetic field, and an inserted rectal temperature sensor.

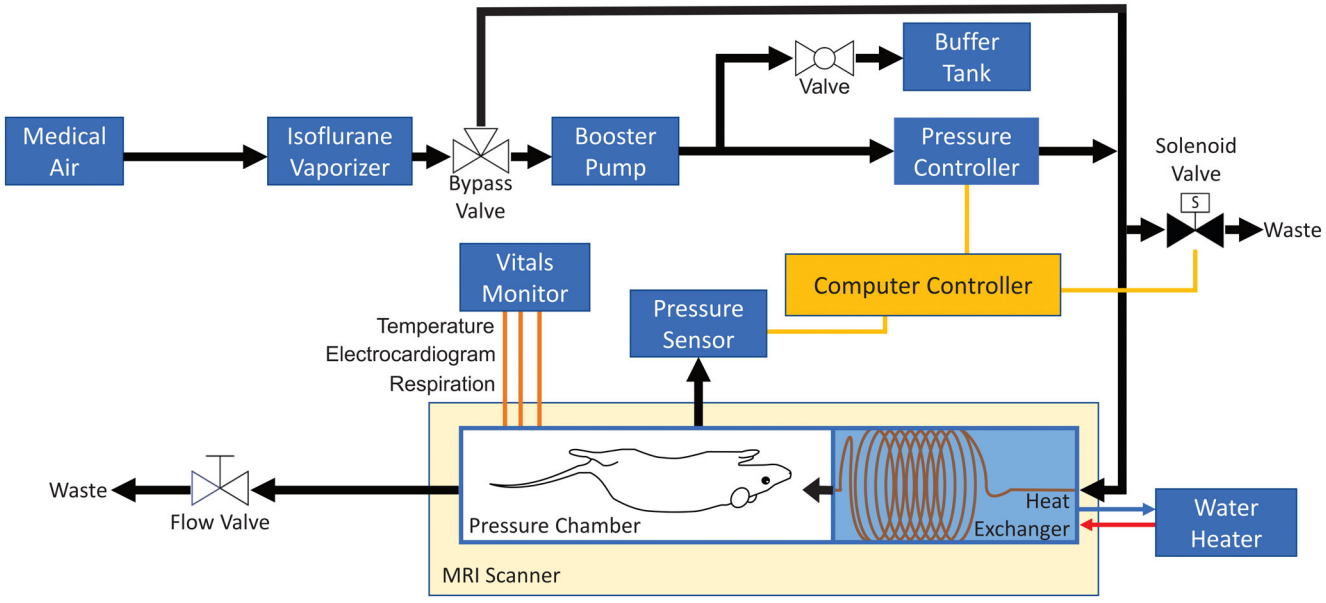

FIGURE 1 Schematic of the chamber and pressurization system. The air pathway is indicated by black arrows, electronic connections are indicated by yellow lines, vital monitoring wiring is indicated by orange lines, and hot water is indicated by a red arrow, whereas cold water is indicated by a blue arrow.

with respiratory motion, a small voltage is induced in the ECG wires, because of the changing magnetic flux through the loop. We used this E-RESP method of respiration monitoring because conventional pneumatic pillows are unsuitable for operation at elevated pressures. Vitals were measured and recorded using the software provided by Small Animal Instruments.

To compensate for heat loss in the animal during imaging, it is not sufficient to warm it by blowing heated air through the bore of the MRI scanner because the RF coil and the pressure chamber occupy most of the MRI bore in our set-up. Therefore, the breathing air is warmed as it enters the chamber with an MRI-compatible heat exchanger that is mounted at the gas inlet end of the pressure chamber. The heat exchanger consists of a small compartment through which warm water is circulated. The breathing gas flows through a 5-m copper tubing coil that is in direct contact with the warm water. The temperature of the warm water can be manually adjusted to maintain the appropriate body temperature of the animal and is typically set to 40°C to raise the pressure chamber temperature by ~3°C.

3 | RESULTS

We successfully compressed two live rats inside the MRI scanner to 7.1 bar absolute for 25 min before decompressing them and maintaining them anesthetized at atmospheric pressure until they succumbed to severe DCS. Real-time MRI scans during this process showed the formation of decompression bubbles in the spinal cord in both rats, but only one is shown here. Figure 3A,left, shows an axial image slice of the thoracic region in the

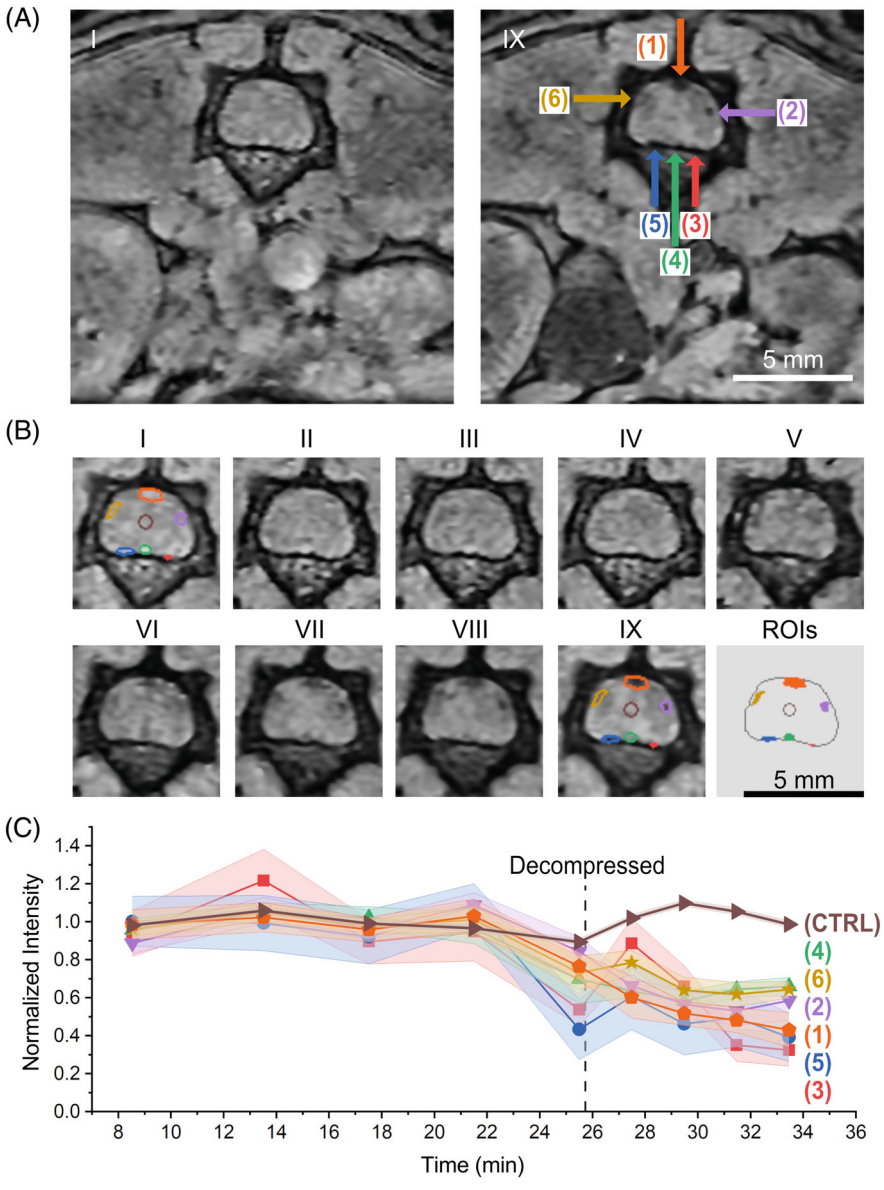

FIGURE 3 MR images of the spinal region of a rat (A) (left) after pressurization to 7.1 bar absolute and (right) 10 min after decompression to 1 bar absolute. The second image shows a gas bubble in the posterior median spinal vein (1), one other suspected gas bubble (2), and several distorted spinal cord regions (3–6). The right third of the spinal cord is darker near (2), possibly indicating hemorrhage. (B) A time series of MRI scans of the spinal cord taken during the experiment are shown. The last panel shows the regions of interest (ROIs) as discussed in Methods, as well as an additional control region (CTRL) located in the center of the ROIs panel. Each region of interest was used to determine the (C) average intensity over the series of images to assess the appearance of bubble formation. The intensity time points indicate the start of the MRI scan. The bubble in the posterior median spinal vein is shown in orange (1), the other suspected bubble is shown in purple (2), a non-bubble control region is shown in brown (CTRL), and other significant spinal cord distortions are shown (3–6).

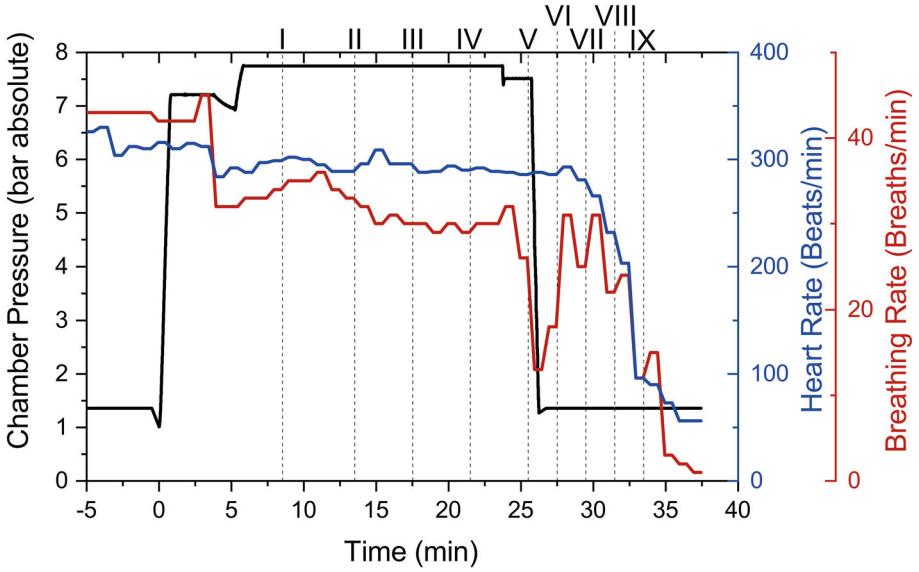

FIGURE 4 Heart rate and respiratory rate of the rat during compression and decompression. The vertical dashed lines indicate the times at which MRI scans were taken and correspond to those shown in Figure 3.

compressed rat, before bubble formation. Figure 3A,right, taken ~10 min after decompression and around the time of the rat's expiration, displays a large gas bubble (1) in the posterior median spinal vein. A smaller gas bubble (2) in the nervous tissue of the spinal cord is also visible. We further note bubble-like entities (3–5) near the anterior region, which may indicate bubble formation between the pia mater and white matter. The right lateral region of the spinal cord (6) is also significantly distorted, but we cannot conclusively associate them with anatomical features of the rat.

The evolution of bubble formation is shown in Figure 3B. The images, while the chamber was compressed (I–IV), showed no significant change, whereas images post decompression (VI–IX), revealed bubbles. Images VI–VIII showed potential left and right lateral vein fracturing occurring that may be responsible for the appearance of hemorrhaging near the second smaller bubble (2). Several regions of interest are shown in Figure 3B-I,B-IX to determine the change in average intensity, including a control region. As indicated in Figure 3C, the average intensity decreases with the formation of a bubble in the posterior median spinal vein (1), in the left lateral most bubble (2), and along the distorted anterior and right lateral regions of the spinal cord (3–6), but not in the non-bubble control region (CTRL).

Continuous monitoring of respiration rate, heart rate, and temperature was conducted during pressure changes, as depicted in Figure 4. Adequate anesthetic depth was successfully maintained throughout the experiment as confirmed via stable vitals. The heart rate stayed around 300 beats per min and the respiratory rate was ~30 to 35 breaths per min until the rat expired.

4 | DISCUSSION AND CONCLUSIONS

Decompression sickness symptoms are closely related to the formation of inert gas bubbles in the body.[3] The exact pathophysiology of how gas bubbles in deeper tissues form, and subsequently dissolve on treatment through recompression remains largely mysterious, as gas bubbles in the spinal cord and similar tissues could only be observed through histopathology until now. Our novel combined pressurization and imaging method allows the observation of decompression gas bubble formation in a live animal under anesthesia in a pressure chamber inside the MRI scanner in real time. We demonstrate a 125 μm voxel resolution for a stack of 30 3.2 cm × 1.6 cm images. This resolution is achieved with four averages for a 4-min scan pre-decompression and two averages for a 2-min scan post-decompression.

We observed the formation of a large bubble with a cross section of ~0.4 mm^2 in the largest vein of the spine, the posterior median spinal vein, and a smaller bubble in another area of the spinal cord. The physical deformations and distortions of the tissue surrounding the bubbles in response to their rapid growth may have led to direct mechanical damage of the tissue and local hemorrhage, eventually leading to the demise of the animal.

In conclusion, we have shown that it is possible to observe the growth of decompression gas bubbles in real time in live rats using MRI in conjunction with a purpose-built pressure cell and life support and monitoring equipment. Using an aggressive compression and decompression protocol that is known to preferentially induce SC-DCS, we were able to observe the formation of gas bubbles in the spinal cord until the animal expired

from the damage. Maintenance and monitoring of anesthesia were possible at isoflurane concentrations that are largely determined by the partial pressure of the anesthetic during the various stages of the experiment. This new capability will enable rigorous testing of many of the assumptions that are made in understanding the pathophysiology of deep-tissue DCS and its treatment though recompression without having to rely solely on histopathology.

ACKNOWLEDGMENTS

This study was funded by the Divers Alert Network, Durham, North Carolina, USA. We thank Angela Yee for her assistance in handling animals during the experiments. The data used this study are openly available.[12]

CONFLICT OF INTEREST STATEMENT

J.C.M. has received a honorarium for participating in the Aerospace Estimation Tool for Hypobaric Exposure Risk Technical Interchange Meeting organized by KBR for NASA, where a small fraction of the data in this paper has been presented.

ORCID

Jens-Christian Meiners https://orcid.org/0009-0000-1506-3133

REFERENCES

1. Brubakk AO, Neuman TS. *Bennett and Elliott's Physiology and Medicine of Diving*. 5th ed. Saunders Limited; 2003.
2. Kutz CJ, Kirby IJ, Grover IR, Tanaka HL. Aviation decompression sickness in aerospace and hyperbaric medicine. *Aerosp Med Hum Perform*. 2023;94:11-17. doi:10.3357/amhp.6113.2023
3. Papadopoulou V, Eckersley RJ, Balestra C, Karapantsios TD, Tang MX. A critical review of physiological bubble formation in hyperbaric decompression. *Adv Colloid Interface*. 2013;191:22-30. doi:10.1016/j.cis.2013.02.002
4. Møllerløkken A, Blogg SL, Doolette DJ, Nishi RY, Pollock NW. Consensus guidelines for the use of ultrasound for diving research. *Diving Hyperb Med*. 2016;46:26-32.
5. Doolette DJ. Venous gas emboli detected by two-dimensional echocardiography are an imperfect surrogate endpoint for decompression sickness. *Diving Hyperb Med*. 2015;46:4-10.
6. Palmer AC. Nature and incidence of bubbles in the spinal cord of decompressed goats. *Undersea Hyperb Med*. 1997;24:193-200.
7. Lillo RS, MacCallum ME. Decompression comparison of N2 and O2 in rats. *Undersea Biomed Res*. 1991;18:317-331.
8. Bradski G. The OpenCV library. *Dr Dobb's J Software Tools*. 2000;25(11):120, 122-125.
9. Harris CR, Millman KJ, van der Walt SJ, et al. Array programming with NumPy. *Nature*. 2020;585:357-362. doi:10.1038/s41586-020-2649-2
10. Virtanen P, Gommers R, Oliphant TE, et al. Author correction: SciPy 1.0: fundamental algorithms for scientific computing in python. *Nat Methods*. 2020;17:261-272. doi:10.1038/s41592-019-0686-2
11. Buades A, Coll B, Morel JM. Non-local means denoising. *IPOL*. 2011;1:208-212. doi:10.5201/ipol.2011.bcm_nlm
12. [dataset]Alvarado R, Scheven UM, Meiners J-C. Raw data for real-time imaging of decompression gas bubble growth in the spinal cord of live rats. *Univ Michigan – Deep Blue*. 2024. doi:10.7302/bb4t-mf19
13. Eisenkraft JB. Anesthesia vaporizers. In: Ehrenwerth J, Eisenkraft JB, Berry JM, eds. *Anesthesia Equipment St*. W.B. Saunders; 2021:66-69. doi:10.1016/b978-0-323-67279-5.00003-0

How to cite this article: Alvarado R, Scheven UM, Meiners J-C. Real-time imaging of decompression gas bubble growth in the spinal cord of live rats. *Magn Reson Med*. 2024;92:1632-1637. doi: 10.1002/mrm.30128